Chemical Science

ROYAL SOCIETY OF CHEMISTRY

EDGE ARTICLE

View Article Online
View Journal | View Issue

Cite this: *Chem. Sci.*, 2023, **14**, 4647

All publication charges for this article have been paid for by the Royal Society of Chemistry

Received 14th December 2022
Accepted 5th April 2023

DOI: 10.1039/d2sc06869a

rsc.li/chemical-science

Effect of modulator ligands on the growth of Co_2(dobdc) nanorods†

Nina S. Pappas and Jarad A. Mason *

Control over the size, shape, uniformity, and external surface chemistry of metal–organic framework nanocrystals is important for a wide range of applications. Here, we investigate how monotopic modulators that mimic the coordination mode of native bridging ligands affect the growth of anisotropic Co_2(dobdc) (dobdc^{4-} = 2,5-dihydroxy-1,4-benzenedicarboxylic acid) nanorods. Through a combination of transmission electron microscopy (TEM) and nuclear magnetic resonance spectroscopy (NMR) studies, nanorod diameter was found to be strongly correlated to the acidity of the modulator and to the degree of modulator incorporation into the nanorod structure. Notably, highly acidic modulators allowed for the preparation of sub-10 nm nanorods, a previously elusive size regime for the M_2(dobdc) family. More broadly, this study provides new insights into the mechanism of modulated growth of metal–organic framework nanoparticles.

Introduction

Leveraging the porosity and tunability of metal–organic frameworks within a size regime that is appropriate for many applications in separations and medicine requires the synthesis of uniform nanocrystals with tailored sizes and shapes.[1] Because of their small size, metal–organic framework nanocrystals feature rapid guest uptake and release kinetics and large external surfaces that can be manipulated independently from internal micropore surfaces to augment material properties.[2] Though there has been substantial progress in expanding the structural and compositional diversity of frameworks that can be synthesized in nanocrystalline form, much remains to be understood about how different synthetic parameters influence the size, shape, and defect structure of metal–organic framework nanocrystals.[3] Moreover, the synthesis of sub-20 nm nanocrystals—a length scale that facilitates the dispersion of metal–organic frameworks in the thin selective layers of commercially viable separation membranes and that includes the diameters of typical proteins[4]—without compromising crystallinity, porosity, or control over particle morphology is an ongoing synthetic challenge.

Coordination modulation, which involves the addition of molecules—often monotopic carboxylic acids—that compete with bridging organic ligands for metal centers is one of the most widely employed approaches for synthesizing metal–organic framework nanocrystals because it offers the ability to simultaneously control particle size, shape, and surface structure.[5] Specifically, monotopic modulators have been proposed to regulate nanoparticle growth in two ways: (1) by capping the surface of growing nanoparticles, and (2) by interfering with bridging ligand deprotonation. Recently, a so-called "seesaw model" was proposed to unify these two regulatory mechanisms.[6] In this model, modulators act primarily as capping ligands when added at low, sub-stoichiometric concentrations by inhibiting nanoparticle growth to drive the formation of smaller particles. When the concentration of a modulator is increased beyond a system-dependent threshold, changes to the proton activity in solution begin interfering with the deprotonation of bridging ligands, causing the nanoparticle size to increase. This seesaw trend has been observed for several common metal–organic frameworks, including UiO-66, MIL-125-NH_2, ZIF-8 and HKUST 1.[7] Furthermore, utilizing modulators that mimic the binding motif of bridging ligands can facilitate size and shape modulation for certain frameworks.[8] Though these studies provide important insights into the modulator-directed growth of metal–organic framework nanoparticles, it is often still challenging to design modulators that direct the formation of nanoparticles with specific characteristics. This is particularly true for anisotropic metal–organic frameworks, for which modulated syntheses are less developed.[5e,f]

Herein, we investigate modulated syntheses of Co_2(dobdc) (dobdc^{4-} = 2,5-dihydroxy-1,4-benzenedicarboxylic acid), which is a member of one of the most well-studied series of anisotropic metal–organic frameworks (M-MOF-74, M_2(dobdc); M = Mg, Mn, Fe, Co, Ni, Cu, Zn).[9] These frameworks feature hexagonal, one-dimensional pore channels lined with a high density of exposed metal centers that lead to strong, selective gas

Department of Chemistry and Chemical Biology, Harvard University, Cambridge, MA, 02138, USA. E-mail: mason@chemistry.harvard.edu

† Electronic supplementary information (ESI) available. See DOI: https://doi.org/10.1039/d2sc06869a

adsorption and interesting reactivity.[10] Several syntheses of M_2(dobdc) nanoparticles have been reported that, depending on the exact conditions, produce both ill-defined particles without uniform surface facets or nanorods with a range of sizes and aspect ratios (Fig. 1).[11,12] In particular, salicylic acid—which is a monotopic analogue of H_2dobdc with the same metal-binding motif—can be used to synthesize nanorods as small as 20 nm in diameter.[12e] In order to better understand the role of modulators in the synthesis of M_2(dobdc) nanorods and to target nanorods of even smaller diameter, we examined how functionalized derivatives of salicylic acid impact the growth of Co_2(dobdc), hypothesizing that modulators with greater acidity (lower pK_a values) would serve as more effective capping ligands by more rapidly trapping growing nanorods and therefore producing smaller nanorods.

Results and discussion

We selected a library of salicylic acid derivatives that spanned a range of acidities to control the concentration of deprotonated modulator that would be present during the initial stages of nanorod nucleation and growth (Fig. 2b). The Co analogue of M_2(dobdc) was chosen because of its tendency to crystallize into particles with well-defined surface facets.[5g,12d–g,i] For all salicylic acid-based modulators, uniform Co_2(dobdc) nanorods were successfully synthesized through solvothermal reactions with a 1 : 1 ratio of modulator to H_2dobdc and, as anticipated, average nanorod diameters—as measured by transmission electron microscopy (TEM)—were strongly correlated to the pK_a of the carboxylic acid functional group on the modulator (Fig. 2b). Specifically, salicylic acid derivatives with higher acidity produced nanorods with smaller diameters, providing access to a previously elusive size regime for M_2(dobdc) nanorods. Though the identity of the modulator had a strong influence on nanorod diameter, there was minimal variation in nanorod lengths (Fig. S21†).

Notably, the use of 4-trifluoromethylsalicylic acid (pK_a = 3.44) as a modulator produced nanorods with an average diameter of just 8.1 ± 1.7 nm, which corresponds to frameworks containing only 5 ± 1 pore channels across. Even in this small size regime, the activated nanorods had an internal BET surface area of 1250 $m^2\ g^{-1}$, which is substantially higher than previous reports of Co_2(dobdc) nanorods (669–874 $m^2\ g^{-1}$)[12e] and is comparable to literature values of bulk Co_2(dobdc) (1080–1438 $m^2\ g^{-1}$).[13] With the exception of nanorods synthesized with 4-bromosalicylic acid (1000 $m^2\ g^{-1}$), all modulators produced nanorods with surface areas in the range of 1200 to 1300 $m^2\ g^{-1}$. These internal surface areas match those reported for bulk Co_2(dobdc), suggesting that the nanorods have minimal internal defects and that the pores and exposed metal centers are not obstructed by excess modulator or bridging ligand. Indeed, CO_2 isotherms at 298 K are also comparable to those of bulk Co_2(dobdc),[9d] with 1 bar CO_2 capacities of 5.8, 5.9 and 6.6 mmol g^{-1} measured for nanorods synthesized with 4-trifluoromethylsalicylic acid, 4-fluorosalicylic acid and 4-methoxysalicylic acid modulators, respectively (Fig. S36†). These gas uptake capacities further highlight the quality of the Co_2(dobdc) nanorods synthesized with salicylic acid modulators, which stands in contrast to many metal–organic framework nanoparticle syntheses—particularly those based on the rapid deprotonation of bridging ligands—that often lead to high defect contents and reduced gas uptake at strong adsorption sites.

In order to gain deeper insight into the modulation mechanism, the degree of modulator incorporation into the synthesized nanorods was quantified by ^{1}H NMR of digested samples after extensive washing to remove any weakly bound

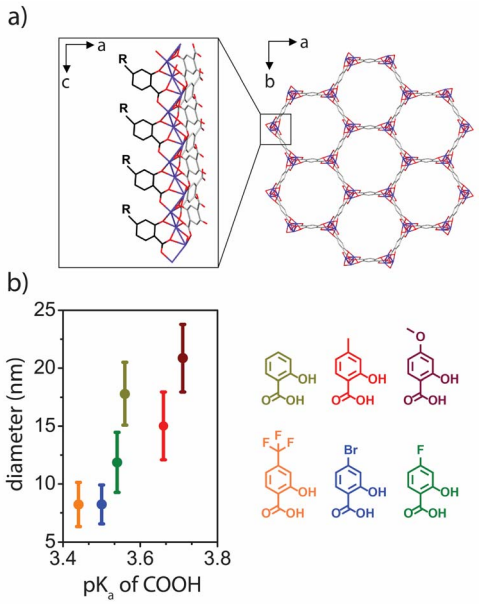

Fig. 2 (a) Crystal structure of Co_2(dobdc) highlighting how monotopic modulators that mimic the coordination mode of dobdc bridging ligands could cap its external surface. Grey/black, red, and purple rods correspond to C, O, and Co atoms, respectively; H atoms are omitted for clarity. (b) The average diameters of Co_2(dobdc) nanorods synthesized in the presence of 1 equivalent of each salicylic acid-based modulator as measured by TEM.

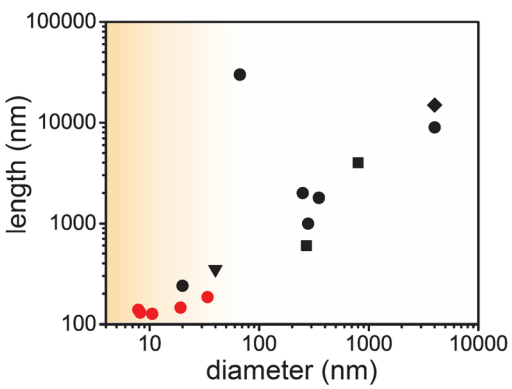

Fig. 1 Summary of lengths and diameters that can be accessed for M_2(dobdc) nanorods, with black squares, diamonds, circles, and triangles, representing previously reported nanorods for M = Mg,[12b,h] M = Mn,[12f] M = Co,[5g,12d–g,i] and M = Zn,[12c] respectively. Red circles represent the Co_2(dobdc) nanorods reported in this work.

modulators. As anticipated, the amount of modulator present was directly correlated with modulator acidity, with the most acidic modulators incorporated to a greater extent than modulators with lower acidities. Though monotopic ligands have been found to incorporate into other metal–organic frameworks as internal defects—most notably for the UiO-66 series of frameworks[14]—the consistent surface areas and CO_2 adsorption capacities of the Co_2(dobdc) nanorods reported here suggest that most of the incorporated modulators are present on the external surfaces of the particles as capping ligands. Indeed, if all of the modulators are assumed to be present on the external surfaces of the nanorods, then the calculated surface coverage does not exceed 100% for any of the modulator ligands (Fig. 3a; see ESI† for additional details about surface coverage model). In addition, we observed an inverse correlation between the degree of modulator surface coverage and the amount of formate incorporated into the nanorod (Fig. S60†), which suggests that the modulators compete with formate—likely produced by DMF hydrolysis during synthesis[5d]—to cap a growing nanorod. The presence of formate and modulator on the external surfaces of the nanorods is also supported by differences in colloidal stability. For instance, nanorods prepared using 4-methoxysalicylic acid which has the lowest modulator surface coverage and highest formate surface coverage, exhibit the best colloidal stability in water (Fig. S8, S9 and S43†), while nanorods prepared with 4-trifluoromethylsalicylic acid, which have highest modulator incorporation, exhibit the best colloidal stability in toluene (Fig. S10†).

To further investigate the location of the incorporated modulators, we performed a post-synthetic ligand exchange experiment. Specifically, nanorods were first prepared with salicylic acid as a modulator, then 4-trifluoromethylsalicylic acid was added to the reaction solution for an additional 24 hours. Importantly, the pre- and post-ligand exchange nanorods display the exact same surface areas (Fig. 4a) and size distributions (Fig. 4c), but digestion NMR (Fig. 4d) shows that

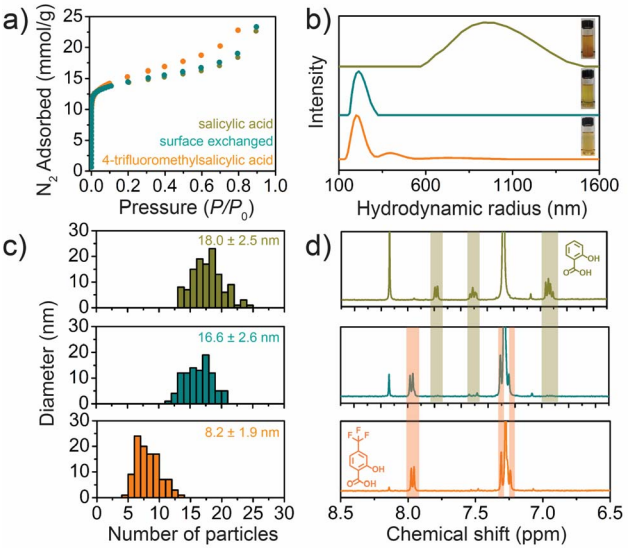

Fig. 4 (a) 77 K N_2 isotherms, (b) dynamic light scattering spectra of toluene solutions, (c) size distributions, and (d) NMR spectra after acid digestion for Co_2(dobdc) nanorods synthesized directly with salicylic acid (yellow) or 4-trifluoromethylsalicylic acid (orange) or synthesized with salicylic acid followed by ligand exchange with 4-trifluoromethylsalicylic (teal).

only 4-trifluoromethylsalicylic acid is present after exchange—indicating that the original salicylic acid modulators are completely exchanged. Moreover, while the quantity of 4-trifluoromethylsalicylic acid modulators incorporated into the nanorods after ligand exchange is slightly higher than the amount of salicylic acid modulators that were originally present, the total amount of modulator and formate remains constant (Table S1†), suggesting that 4-trifluoromethylsalicylic acid can exchange with both salicylic acid and formate.

Nearly identical 77 K N_2 adsorption isotherms before and after ligand exchange (teal and gold curves in Fig. 4a) suggest that the vast majority of the salicylic acid modulators are present on the external surface, as internal defects are known to impact surface areas and pore volumes, particularly for ligands with very different steric profiles.[15] Moreover, we observed significant changes to the colloidal stability of the nanorods after ligand exchange, and dispersibility should be mostly—if not entirely—governed by the external surface chemistry of the nanorods. Specifically, the original nanorods rapidly aggregate in toluene, while the post-ligand exchange nanorods form much more stable dispersions (Fig. 4b). Indeed, the colloidal stability of the post-exchange nanorods matched that of nanorods synthesized directly with 4-trifluoromethylsalicylic acid modulators, even though the direct synthesis leads to much smaller nanorods. While it is possible that some of the modulators incorporate into the internal structure of the framework, these results collectively provide strong evidence that a large fraction of the modulators—and likely the majority—are present on the external surface. We hypothesize that differences in the dominant location of organic modulators for Co_2(dobdc) nanorods

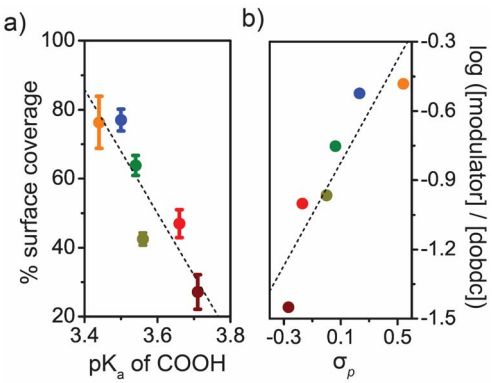

Fig. 3 (a) The external surface coverage of salicylic acid-based modulators is calculated by assuming modulators are only present on the external surface of each nanorod. (b) Hammett plot for Co_2(dobdc) nanorods synthesized in the presence of 1 equivalent of salicylic acid modulator.

compared to other modulated metal–organic framework syntheses can be attributed to (1) the small diameters and large external surface areas of the nanorods, (2) one-dimensional pore channels that inhibit lateral diffusion of reagents, and (3) bridging organic ligands that are closely packed along one dimension.

The observed trends in modulator surface coverage and particle size are consistent with nanorod growth operating under kinetic control, where modulators with higher acidities provide a higher concentration of deprotonated ligands to cap growing particles, rather than thermodynamic control, where modulators with lower acidities would be expected to more strongly cap growing nanorods though the formation of stronger metal–modulator bonds. The kinetic control of nanoparticle growth has been described as a balance between the steady–state equilibrium of modulators coordinating to the surface and the diffusion rate of metal ions to the nanoparticle surface.[6] Size modulation is achieved when the steady–state equilibrium of modulator coordination overwhelms the surface of the nanoparticle and depletes the local metal ion concentration due to the presence of a high concentration of deprotonated modulator. By utilizing modulators with various acidities, the position of this steady–state equilibrium can be altered to control the rate of kinetic capping and, consequently, the size of the metal–organic framework nanoparticles. Interestingly, our observed modulator-dependant size trends for Co_2(dobdc) differ from previous reports that found more acidic benzoic acid derivatives produced larger MIL-101(Cr) nanoparticles with less incorporation of the modulator into the framework.[5a] We suspect that the different trends observed for MIL-101(Cr) are likely due to a number of factors, including the choice of reaction solvent (water *versus* DMF) and the large difference in modulator concentration and overall reaction concentration used during synthesis.

To investigate if modulators impact Co_2(dobdc) nanorod growth through pH modulation in addition to acting as capping ligands, syntheses were also performed using three benzoic acid-based modulators (benzoic acid, 4-trifluoromethylbenzoic acid, and 4-methoxybenzoic acid) that should provide similar pH modulation effects as their salicylic acid counterparts but lack the same metal-binding motif for nanoparticle capping. Rather than directing the formation of nanorods, all three benzoic acid derivatives produced irregular aggregates of globular Co_2(dobdc) nanoparticles with similar particle sizes and no detectable modulator incorporation (Fig. S4, S26 and S57–S59†). This result highlights the importance of mimicking the bridging ligand binding motif for modulating the growth of Co_2(dobdc)—at least in sub-20 nm size regime—and suggests that pH modulation has minimal impact on the size modulation of nanorods under the reactions conditions investigated in this work.

The dominance of a capping mechanism is further supported by a Hammett analysis (Fig. 3b), where the impact of substituent (R) electronic effects on the modulator-metal coordination reaction kinetics can be probed by plotting the relative modulator concentration in the synthesized nanorods against the substituent constant σ_p.[16] The slope of this plot indicates the degree to which the electronic nature of the substituents (σ_p) affects the reaction kinetics. The linear relationship observed for Co_2(dobdc) nanorods indicates that all modulator complexation reactions proceed *via* the same mechanism with a strong dependence on the ionization of the carboxylic acid, further supporting the hypothesis that lower pK_a modulators act as more effective capping ligands because they are more readily deprotonated (Fig. 3b).

To probe how the presence of different modulators affect particle growth, a competition study was performed where Co_2(dobdc) nanorods were synthesized in the presence of both 4-trifluoromethylsalicylic acid (pK_a = 3.44) and 4-methoxysalicylic acid modulators (pK_a = 3.71). The prepared nanorods displayed a single size distribution (average diameter of 11.4 nm) that is more closely aligned with the size of the nanorods produced using 4-trifluoromethylsalicylic acid (Fig. S17 and S23†), and 4-trifluoromethylsalicylic acid was the only modulator observed in a digested sample of the washed nanorods (Fig. S44†). This provides additional support for the hypothesis that the observed size modulation is the result of rapid kinetic trapping from deprotonated modulators capping the surface of growing nanoparticles.

To examine if increasing the concentration of modulator in the synthesis would further enhance kinetic trapping or initiate a transition to pH modulation, Co_2(dobdc) nanorods were synthesized with varying equivalents (1, 1.5, 2, 3) of either 4-trifluoromethylsalicylic acid, salicylic acid, or 4-methoxysalicylic acid. When the pK_a of the modulator was closely matched to that of the dobdc bridging ligand—as is the case for salicylic acid—we observed a seesaw relationship between modulator concentration and nanorod diameter, with 1.5 equivalents of salicylic acid producing particles with the smallest diameter (15.3 nm ± 2.3 nm) (Fig. S61†). This is consistent with a capping mechanism dominating modulation at low concentrations and pH changes—or the degree of modulator and bridging ligand deprotonation—dominating at higher concentrations.[6,7] Interestingly, when the pK_a of the modulator was higher or lower than the bridging ligand—as is the case for 4-methoxysalicylic acid and 4-trifluoromethylsalicylic acid, respectively—modulator concentration had minimal effect on nanorod diameter even though the degree of modulator incorporation increased with increasing modulator concentration (Fig. S61†). This suggests that changes to modulator capping and pH effects may offset one another as the modulator concentration is increased. Specifically, when the pK_a of the modulator is similar to the bridging ligand, pH modulation affects the concentration of both deprotonated ligands, leading to a seesaw trend with nanoparticle size inversely proportional to modulator concentration at low concentrations and directly proportional at high concentrations. However, our data suggests that when the pK_a of the modulator is either above or below the pK_a of the bridging ligand, changes in solution pH—as a result of increasing modulator content—no longer affect both ligands in the same way. These offsetting effects could then explain why the

nanorod size does not have a strong dependence on modulator concentration.

Conclusions

The foregoing results demonstrate how the acidity of organic modulators can be manipulated to control the growth of anisotropic metal–organic framework nanoparticles in a predictable fashion. In particular, more rapid capping through the use of modulators with higher acidities provides access to an ultrasmall size regime—below 10 nm—for Co_2(dobdc) nanorods and offers insight into the role of modulators in the synthesis of metal–organic frameworks. These insights should provide new opportunities for controlling the size, shape, and surface chemistry of a wider range of metal–organic framework nanoparticles.

Data availability

Details of nanorod syntheses, powder X-ray diffraction, thermogravimetric analysis, dynamic light scattering, transmission electron microscopy, surface area and gas adsorption measurements, and NMR experiments are included in the ESI.† Other data are available from the corresponding author upon reasonable request.

Author contributions

N. S. P. and J. A. M. conceived the project. N. S. P. carried out all nanoparticle syntheses and performed all characterization experiments. N. S. P. and J. A. M. analyzed the data and wrote the manuscript.

Conflicts of interest

There are no conflicts to declare.

Acknowledgements

This research was partially supported by the Arnold and Mabel Beckman Foundation through a Beckman Young Investigator grant to J. A. M. and by a Multidisciplinary University Research Initiative, sponsored by the Department of the Navy, Office of Naval Research, under grant N00014-20-1-2418. This work was performed in part at the Harvard University Center for Nanoscale Systems (CNS); a member of the National Nanotechnology Coordinated Infrastructure Network (NNCI), which is supported by the National Science Foundation under NSF award ECCS-2025158. We thank Dr A. H. Slavney and Dr M. B. Wenny for helpful discussions and J. Tucker and J. Gonzales for experimental assistance.

References

1 (*a*) A. Carné, C. Carbonell, I. Imaz and D. Maspoch, *Chem. Soc. Rev.*, 2011, **40**, 291–305; (*b*) J. Della Rocca, D. Lin and W. Lin, *Acc. Chem. Res.*, 2011, **44**, 957–968; (*c*) H. Furukawa, K. E. Cordova, M. O'Keeffe and O. M. Yaghi, *Science*, 2013, **341**, 1230444; (*d*) M. Sindoro, N. Yanai, A. Lee and S. Granick, *Acc. Chem. Res.*, 2014, **47**, 459–469; (*e*) M. Giménez-Marqués, T. Hidalgo, C. Serre and P. Horcajada, *Coord. Chem. Rev.*, 2016, **15**, 342–360; (*f*) S. Wang, M. McGuirk, D. d'Anquino, J. A. Mason and C. A. Mirkin, *Adv. Mater.*, 2018, **30**, 1800202; (*g*) S. Kuyuldar, D. T. Genna and C. Burda, *J. Mater. Chem. A.*, 2019, **7**, 21545–21576; (*h*) X. Cai, Z. Xie, D. Li, M. Kassymova, S. Zang and H. Jiang, *Coord. Chem. Rev.*, 2020, **417**, 213366; (*i*) E. Ploetz, H. Engelke, U. Lächelt and S. Wuttke, *Adv. Funct. Mater.*, 2020, **30**, 1909062; (*j*) X. Xiao, L. Zou, H. Pang and Q. Xu, *Chem. Soc. Rev.*, 2020, **49**, 301–331.

2 (*a*) I. Abánades Lázaro, S. Haddad, J. Rodrigo-Muñoz, R. J. Marshall, B. Sastre, V. del Pozo, D. Fairen-Jimenez and R. S. Forgan, *ACS Appl. Mater. Interfaces*, 2008, **10**, 31146–31157; (*b*) S. Wang, W. Morris, Y. Liu, M. McGuirk, Y. Zhou, J. T. Hupp, O. K. Farha and C. A. Mirkin, *Angew. Chem., Int. Ed.*, 2015, **54**, 14738–14742; (*c*) B. Rungtaweevoranit, Y. Zhao, K. M. Choi and O. M. Yaghi, *Nano Res.*, 2016, **9**, 47–58; (*d*) I. A. Lázaro, S. Haddad, S. Sacca, C. Orellana-Tavra, D. Fairen-Jimenez and R. S. Forgan, *Chem*, 2017, **2**, 561–578.

3 (*a*) N. Stock and S. Biswas, *Chem. Rev.*, 2012, **112**, 933–969; (*b*) M. B. Majewski, H. Noh, T. Oslamoglu and O. K. Farha, *J. Mater. Chem. A.*, 2018, **6**, 7338–7350.

4 (*a*) T. Rodenas, I. Luz, G. Prieto, B. Seoane, H. Miro, C. Corma, F. Kapteijin, F. Llabrés I Xamena and J. Gascon, *Nat. Mater.*, 2015, **14**, 48–55; (*b*) M. Shete, P. Humar, J. E. Bachman, X. Ma, Z. P. Smith, W. Xu, K. Andre Mkhoyan, J. R. Long and M. Tsapatsis, *J. Membr. Sci.*, 2018, **549**, 312–320; (*c*) Q. Qian, P. A. Asinger, M. Joo Lee, G. Han, K. Mizrahi Rodriguez, S. Lin, F. M. Benedetti, A. X. Wu, W. Seok Chi and Z. Smith, *Chem. Rev.*, 2020, **120**, 8161–8266.

5 (*a*) D. Jiang, A. D. Burrows and K. J. Edler, *CrystEngComm*, 2011, **13**, 6916–6919; (*b*) Z. Hu, I. Castano, S. Wang, Y. Wang, Y. Peng, Y. Qian, C. Chi, X. Wang and D. Zhau, *Cryst. Growth Des.*, 2016, **16**, 2295–2301; (*c*) W. Morris, S. Wang, D. Cho, E. Auyeung, P. Li, O. K. Farha and C. A. Mirkin, *ACS Appl. Mater. Interfaces*, 2017, **9**, 33413–33418; (*d*) R. S. Forgan, *Chem. Sci.*, 2020, **11**, 4546–4562; (*e*) B. L. Bonnett, S. Ilic, K. Flint, M. Cai, X. Yang, H. D. Cornell, A. Taylor and A. J. Morris, *Inorg. Chem.*, 2021, **60**, 10439–10450; (*f*) K. Colwell, M. Jackson, R. Torres-Gavosto, S. Jawahery, B. Vlaisavljevich, J. Falkowki, B. Smit, S. Weston and J. Long, *J. Am. Chem. Soc.*, 2021, **143**, 5044–5052.

6 C. Marshall, S. Staudhammer and C. Brozek, *Chem. Sci.*, 2019, **10**, 9396–9408.

7 (*a*) S. Hu, M. Liu, X. Guo, K. Li and C. Han, *Cryst. Growth Des.*, 2017, **17**, 6586–6595; (*b*) C. R. Marshall, E. E. Timmel, S. A. Staudhammer and C. K. Brozek, *Chem. Sci.*, 2020, **11**, 11539–11547.

8 (*a*) K. Suresh, A. P. Kalenak, A. Sotuyo and A. J. Matzger, *Chem. – Eur. J.*, 2022, **28**, 1–8; (*b*) K. Suresh, D. Aulakh,

J. Purewal, D. J. Siegel, M. Veenstra and A. J. Matzger, *J. Am. Chem. Soc.*, 2021, **143**, 10727–10734.

9 (*a*) P. D. C. Dietzel, Y. Morita, R. Blom and H. Fjellvåg, *Angew. Chem., Int. Ed.*, 2005, **44**, 6354–6358; (*b*) N. L. Rosi, J. Kim, M. Eddaoudi, B. Chen, M. O'Keeffee and O. M. Yaghi, *J. Am. Chem. Soc.*, 2005, **127**, 1504–1518; (*c*) P. D. C Dietzel, B. Panella, M. Hirscher, R. Blom and H. Fjellvåg, *Chem. Commun.*, 2006, 959–961; (*d*) S. R. Caskey, A. G. Wong-Foy and A. J. Matzger, *J. Am. Chem. Soc.*, 2008, **130**, 10870–10871; (*e*) W. Zhou, H. Wu and T. Yildirim, *J. Am. Chem. Soc.*, 2008, **130**, 15268–15269; (*f*) E. D. Bloch, L. J. Murray, W. L. Queen, S. Chavan, S. N. Maximoff, J. P. Bigi, R. Krishna, V. Peterson, F. Grandjean, G. J. Long, B. Smit, S. Bordiga, C. M. Brown and J. R. Long, *J. Am. Chem. Soc.*, 2011, **133**, 14814–14822; (*g*) R. Sanz, F. Martínez, G. Orcajo, L. Wojtas and D. Briones, *Dalton Trans.*, 2013, **42**, 2392–2398.

10 (*a*) P. D. C. Dietzel, V. Besikiotis and R. Blom, *J. Mater. Chem.*, 2009, **19**, 7362–7370; (*b*) J. A. Mason, K. Sumida, Z. Herm, R. Krishna and J. R. Long, *Energy Environ. Sci.*, 2011, **4**, 3030–3040; (*c*) K. Sumida, C. M. Brown, Z. R. Herm, S. Chavan, S. Bordiga and J. R Long, *Chem. Commun.*, 2011, **47**, 1157–1159; (*d*) Y.-S. Bae, C. Y. Lee, K. C. Kim, O. K. Farha, P. Nickias, J. T. Hupp, S. T. Nguyen and R. Q. Snurr, *Angew. Chem., Int. Ed.*, 2012, **8**, 1857–1860; (*e*) S. J. Geier, J. A. Mason, E. D. Bloch, W. L. Queen, M. R. Hudson, C. M. Brown and J. R. Long, *Chem. Sci.*, 2013, **4**, 2054–2061; (*f*) E. D. Bloch, M. R. Hudson, J. A. Mason, S. Chavan, V. Crochellà, J. D. Howe, K. Lee, A. L. Dzubak, W. L. Queen, J. M. Zadrozny, S. J. Geier, L.-C. Lin, L. Gagliardi, B. Smit, J. B. Neaton, S. Bordiga, C. M. Brown and J. R. Long, *J. Am. Chem. Soc.*, 2014, **136**, 10752–10761; (*g*) D. J. Xiao, E. D. Bloch, J. A. Mason, W. L. Queen, M. R. Hudson, N. Planas, J. Borycz, A. L. Dzubak, P. Verma, K. Lee, F. Bonino, V. Crocellà, J. Yano, S. Bordiga, D. G. Truhlar, L. Gagliardi, C. M. Brown and J. R. Long, *Nat. Mater.*, 2014, **6**, 590–595.

11 (*a*) T. Bae and J. R. Long, *Energy Environ. Sci.*, 2013, **6**, 3565–3569; (*b*) M. Díaz-García, A. Mayoral, I. Díaz and M. Sánchez-Sánchez, *Cryst. Growth Des.*, 2014, **14**, 2479–2487; (*c*) J. E. Bachman, Z. P. Smith, T. Li, T. Xu and J. R. Long, *Nat. Mater.*, 2016, **15**, 845–849; (*d*) J. Campbell and B. Tokay, *Microporous Mesoporous Mater.*, 2017, **251**, 190–199; (*e*) J. Wang, Y. Fan, H. Lee, C. Yi, C. Cheng, X. Zhao and M. Yang, *ACS Appl. Nano Mater.*, 2018, **1**, 3747–3753; (*f*) E. Roh, I. Subiyanto, W. Choi, Y. Cheol Park, C. Cho and H. B. Kim, *Korean Chem. Soc.*, 2021, **42**, 459–462.

12 (*a*) E. Haque and S. Jhuang, *Chem. Eng. J.*, 2011, **3**, 866–872; (*b*) X. Wu, Z. Bao, B. Yuan, J. Wang, Y. Sun, H. Luo and S. Deng, *Microporous Mesoporous Mater.*, 2013, **180**, 114–122; (*c*) P. Pachfule, D. Shinde, M. Majumder and W. Xu, *Nat. Chem.*, 2016, **8**, 718–724; (*d*) J. Chen, X. Mu, M. Du, Y. Lou and Y. Inorg, *Chem. Commun.*, 2017, **84**, 241–245; (*e*) W. Yan, Z. Guo, H. Xu, Y. Lou, J. Chen and Q. Li, *Mater. Chem. Front.*, 2017, **1**, 1324–1330; (*f*) S. H. Kim, Y. J. Lee, D. H. Kim and J. Y. Lee, *ACS Appl. Mater. Interfaces*, 2018, **10**, 660–667; (*g*) L. Zou, C. Hou, Z. Liu, H. Pang and Q. Xu, *J. Am. Chem. Soc.*, 2018, **140**, 15393–153401; (*h*) C. Wu, L. Chou, L. Long, X. Si, W. Lo, C. Tsung and T. Li, *ACS Appl. Mater. Interfaces*, 2019, **11**, 35820–35826; (*i*) Y. Yan, J. Ma and L. Guo, *Talanta*, 2019, **205**, 210138.

13 (*a*) W. L. Queen, M. R. Hudson, E. D. Bloch, J. A. Mason, M. I. Gonzalez, J. S. Lee, D. Gygi, J. D. Howe, K. Lee, T. A. Darwish, M. James, V. K. Peterson, S. J. Teat, B. Smit, J. B. Neaton, J. R. Long and C. M. Brown, *Chem. Sci.*, 2014, **5**, 4569–4581; (*b*) M. I. Gonzalez, J. A. Mason, E. D. Bloch, S. J. Teat, K. J. Gagnon, G. Y. Morrison, W. L. Queen and J. R. Long, *Chem. Sci.*, 2017, **8**, 4387–4398; (*c*) M. T. Kapelewski, T. Runčevski, J. D. Tarver, H. Z. H. Jiang, K. E. Hurst, P. A. Parilla, A. Ayala, T. Gennett, S. A. FitzGerald, C. M. Brown and J. R. Long, *Chem. Mater.*, 2018, **30**, 8179–8189; (*d*) H. Kim, M. Sohail, K. Yim, Y. Park, D. Chun, H. Kim, S. Han and J. Moon, *ACS Appl. Mater. Interfaces*, 2019, **11**, 7014–7021.

14 (*a*) G. C. Shearer, S. Chavan, S. Bordiga, S. Svelle, U. Olsbye and K. P. Lillerud, *Chem. Mater.*, 2016, **28**, 3749–3761; (*b*) I. A. Lazaro, C. Popescu and F. G. Cirujano, *Dalton Trans.*, 2021, **50**, 11291–11299.

15 (*a*) Y. Fu, A. C. Force, Z. Kang, M. J. Cliffe, W. Cao, J. Yin, L. Gao, Z. Pang, T. He, Q. Chen, Q. Wang, J. R. Long, J. A. Reimer and X. Kong, *Sci. Adv.*, 2023, **9**, 1–9; (*b*) S. Kim, A. Kim, J. W. Yoon, H. Kim and Y. Bae, *Chem. Eng. J.*, 2018, **335**, 94–100; (*c*) D. Wu, W. Yan, H. Xu, E. Zhang and Q. Li, *Inorg. Chim. Acta*, 2017, **460**, 93–98; (*d*) J. A. Villajos, N. Jagorel, S. Reinsch and F. Emmerling, *Front. Mater.*, 2019, **6**, 1–10.

16 L. P. Hammett, *J. Am. Chem. Soc.*, 1937, **59**, 96–103.